Break-seq reveals hydroxyurea-induced chromosome fragility as a result of unscheduled conflict between DNA replication and transcription

Elizabeth A. Hoffman,[1] Andrew McCulley, Brian Haarer, Remigiusz Arnak, and Wenyi Feng

Department of Biochemistry and Molecular Biology, SUNY Upstate Medical University, Syracuse, New York 13210, USA

We have previously demonstrated that in *Saccharomyces cerevisiae* replication, checkpoint inactivation via a *mec1* mutation leads to chromosome breakage at replication forks initiated from virtually all origins after transient exposure to hydroxyurea (HU), an inhibitor of ribonucleotide reductase. Here we sought to determine whether all replication forks containing single-stranded DNA gaps have equal probability of producing double-strand breaks (DSBs) when cells attempt to recover from HU exposure. We devised a new methodology, Break-seq, that combines our previously described DSB labeling with next generation sequencing to map chromosome breaks with improved sensitivity and resolution. We show that DSBs preferentially occur at genes transcriptionally induced by HU. Notably, different subsets of the HU-induced genes produced DSBs in *MEC1* and *mec1* cells as replication forks traversed a greater distance in *MEC1* cells than in *mec1* cells during recovery from HU. Specifically, while *MEC1* cells exhibited chromosome breakage at stress-response transcription factors, *mec1* cells predominantly suffered chromosome breakage at transporter genes, many of which are the substrates of those transcription factors. We propose that HU-induced chromosome fragility arises at higher frequency near HU-induced genes as a result of destabilized replication forks encountering transcription factor binding and/or the act of transcription. We further propose that replication inhibitors can induce unscheduled encounters between replication and transcription and give rise to distinct patterns of chromosome fragile sites.

[Supplemental material is available for this article.]

Chromosome fragile sites (CFSs) were defined cytologically as site-specific gaps, constrictions, or breakage on mammalian metaphase chromosomes (Sutherland 1979). Recent years have seen intense scrutiny of the underlying mechanisms of chromosome fragility as increasing evidence suggests that CFSs are hotspots for genome rearrangements frequently observed in cancer cells (Arlt et al. 2006; Durkin and Glover 2007; Casper et al. 2012; Debatisse et al. 2012). Replication timing analyses suggested that DNA replication fork instability is a potential cause for chromosome fragility (Le Beau et al. 1998; Wang et al. 1998; Hellman et al. 2000; Palakodeti et al. 2004). Recent studies also suggested that, at least in the case of FRA3B and FRA16D (two of the most frequent common fragile sites in the human genome), paucity of replication initiation events is correlated with chromosome fragility (Letessier et al. 2011; Ozeri-Galai et al. 2011). Thus, the mechanism of chromosome fragility at the CFSs still remains unclear—in particular, theories that are capable of explaining why different cell types or replication inhibitors produce distinct spectra of CFSs are still lacking. For instance, it was reported that fibroblasts and lymphocytes from the same individual showed different frequencies of CFSs (Murano et al. 1989). It is thought that differential gene expression plays a role in shaping the chromosome fragility profile under various conditions, suggesting that conflict between replication and gene expression may be an underlying cause of chromosome fragility.

[1]Present address: Department of Biochemistry and Molecular Genetics, University of Virginia Health System, Charlottesville, Virginia 22908, USA

Corresponding author: fengw@upstate.edu

Article published online before print. Article, supplemental material, and publication date are at http://www.genome.org/cgi/doi/10.1101/gr.180497.114. Freely available online through the *Genome Research* Open Access option.

Conflict between replication and transcription is a well-documented phenomenon in both prokaryotes and eukaryotes (Bermejo et al. 2012; Merrikh et al. 2012). Such conflicts, particularly head-on collisions, are generally avoided in most model organisms as recently reviewed (Mirkin and Mirkin 2007). For instance, highly transcribed genes are encoded on the leading strand in most bacterial genomes (Rocha 2002). It was hypothesized that such an organization would ensure the directions of replication and transcription to be codirectional and to avert head-on collisions (Brewer 1988). In those cases in which coincidental transcription and replication are inevitable, cells seem to have evolved mechanisms to resolve these conflicts without any apparent ill consequence. For example, the yeast ribosomal DNA locus also contains a replication fork barrier to specifically halt replication fork progression, thereby averting head-on collisions between the transcription and replication machineries (Brewer and Fangman 1988). Intriguingly, the *Saccharomyces cerevisiae* genome is rather conducive to such potential conflict as the origins of replication (origins hereafter) are preferentially located in intergenic regions between converging transcription units (MacAlpine and Bell 2005; Nieduszynski et al. 2007; Yin et al. 2009). It has also been shown that yeast tRNAs can stall replication forks in a polar fashion (Deshpande and Newlon 1996). Similarly, RNA polymerase II (Pol II) transcribed genes can produce strong pause sites for replication forks (Azvolinsky et al. 2009). How the organism resolves these potential conflicts and maintains fitness is still unclear. Interestingly, in vitro experiments using programmed head-on col-

25:402–412 Published by Cold Spring Harbor Laboratory Press; ISSN 1088-9051/15; www.genome.org

lision between *Escherichia coli* DNA and RNA polymerases indicated that the replication fork is capable of resuming synthesis without collapsing upon collision (Pomerantz and O'Donnell 2010). However, such analysis has not been performed with eukaryotic enzymes where DNA polymerase has a relatively lower speed than the bacterial equivalent and therefore might not fare as well in a collision with the RNA polymerase. Consistent with this notion, mutations in a multitude of pathways that increase the frequency of replication-transcription conflicts can lead to genome instability (Tuduri et al. 2009; Luna et al. 2012; Duch et al. 2013). Here we propose that replication inhibitors can also induce unscheduled conflicts between replication and transcription due to their dual effects on these two processes, leading to DSBs.

We recently examined the dynamics of chromosome fragility in a yeast replication checkpoint mutant, *mec1-1 sml1-1* (*mec1-1* is a lethal mutation that requires the presence of the *sml1-1* allele for survival, hereafter referred to as *mec1* for simplicity), after nucleotide starvation by a potent inhibitor of ribonucleotide reductase, hydroxyurea (HU) (Feng et al. 2011). Using microarray-based simultaneous mapping of single-stranded DNA (ssDNA) and double-strand breaks (DSBs), we observed that chromosomal fragility was preceded by ssDNA formation at the replication forks. However, DSBs were observed at apparently similar frequencies at the replication forks throughout the genome. Moreover, although ssDNA was present at replication forks during exposure to HU, high levels of DSBs were not evident until HU was removed from the cells. These observations prompted the current study in which we asked whether replication forks at certain genomic regions are more prone to breakage than at others, particularly during recovery from HU.

Here we describe an improved methodology named "Break-seq" that combines the previously described DSB mapping by end-repair (Feng et al. 2011) with next generation sequencing technology, a readout that provides unparalleled sensitivity and resolution compared to microarrays (hereafter referred to as "Break-chip"). Break-seq facilitated the detection of DSBs not only during cell recovery from HU, where chromosome breakage was abundant, but also when cells were still exposed to HU where chromosome breakage was below detection by previous methods. We identified breakage hotspots at a wide range of transporter genes, including metal ion transmembrane transporters in *mec1* cells and at stress-response transcriptional factors in *MEC1* cells. Based on these results, we propose that DSBs result from a clash between unstable replication forks and increased transcription at HU-induced genes due to the dual effects of HU on replication and gene transcription.

Results

Break-seq, a universally adaptable DSB mapping method

We previously used Break-chip to map chromosome breakage in the yeast checkpoint mutant *mec1* and demonstrated that HU treatment causes single-stranded DNA (ssDNA) formation at replication forks, which is subsequently converted to DSBs by an unknown mechanism (Feng et al. 2011). However, it is unclear if all ssDNA regions have equal likelihood of becoming DSBs. Moreover, if the DSBs resulted from intrinsic instability of the ssDNA, it is unclear why chromosome breakage is only evident during recovery from HU rather than when cells are still in HU (Feng et al. 2009). To achieve DSB detection with high sensitivity, we developed an improved methodology, Break-seq (Fig. 1A). Briefly, we labeled DNA ends with biotin using the T4 DNA polymerase contained in the End-Repair enzyme mix (End-It, Epicentre), followed by shearing of the chromosomal DNA, capturing labeled double-stranded DNA and constructing libraries using multiplexed Illumina technology. We used the Burrows-Wheeler Aligner (Li and Durbin 2009) or Bowtie 2 (Langmead and Salzberg 2012) to align these sequence reads to the *S. cerevisiae* reference genome (SacCer3) (Supplemental Table S1). We then used MACS (Model-based Analysis of ChIP-seq) to identify genomic regions showing significant levels ($P < 1 \times 10^{-5}$) of end-labeled signals in either a single sample (One-Sample test) or enriched in a sample compared to a control (Two-Sample test) (Zhang et al. 2008).

We first performed a proof-of-concept experiment by digesting a G1-arrested (by α-factor) sample from *mec1* cells with BamHI in vitro (referred to as the $G1^{BamHI}$ sample), followed by Break-seq. We identified 1296 DSBs in the $G1^{BamHI}$ sample with apparently good correlation with the known 1679 BamHI sites in the S288c reference genome based on visual inspection (Fig. 1B). We further demonstrated that 231 of 241 DSBs on four representative chromosomes (II, III, VI, and X) were found within a 1-kb distance from a known BamHI site with a median distance of 217 bp (Supplemental Table S2). This result demonstrated that the Break-seq method identifies bona fide DSBs. It also implies that the average end-repair track length by T4 DNA polymerase is 200–300 bp.

Break-seq permits detection of low levels of DSBs at origins of replication during exposure to HU

We performed two independent experiments (Exp A and B) for *mec1* and one experiment (Exp C) for *MEC1* cells and collected the following samples: (1) cells synchronously released into S phase in the presence of 200 mM HU for 1 h (HU); and (2) cells recovered for 1 h after removal of HU (Recovery). For clarity, hereafter the samples associated with the *MEC1* and *mec1* cells will bear the superscripts "*MEC1*" (as in HU^{MEC1}) and "*mec1*" (as in $Recovery^{mec1}$), respectively. Both the HU^{mec1} samples and the $Recovery^{mec1}$ samples exhibited significant concordance between the two experiments (Fig. 1C; Supplemental Table S3). To compare the DSB profiles between samples, we visualized the sequence reads using SeqMonk (Babraham Bioinformatics, http://www.bioinformatics.babraham.ac.uk/projects/seqmonk/) (Fig. 2A; Supplemental Fig. S1). We also tested if copy number variation in the samples in S phase would produce artifactual DSB signals at the replicated region by performing Break-seq from the G1 samples or "mock" Break-seq without biotinylated nucleotides from the HU samples. Both control samples yielded apparently random signals across the genome (Supplemental Fig. S2). However, we note that some of the signals in the mock Break-seq samples were enriched near origins (Supplemental Fig. S2, black arrows).

Using MACS, we detected 138 and 151 DSB peaks in the HU^{mec1} samples of Exp A and B, respectively, with ~60% concordance (Fig. 2B; Supplemental Table S4). We also detected 103 DSB peaks in the HU^{MEC1} sample (Supplemental Table S4). We compared the locations of these DSBs to those of 626 confirmed or likely OriDB (origin database)-curated origins (http://www.oridb.org; *S. cerevisiae* v2.0.1). The majority of the DSBs in the HU^{mec1} samples, 79% (109 of 138) and 85% (129 of 151) from Exp A and B, overlapped with an origin with the median distance between their mid points being 600 bp and 377 bp, respectively. Similarly, 72% (74 of 103) of DSBs from the HU^{MEC1} sample overlapped with an origin with a median distance of 543 bp. Colocalization of the DSBs and the origins was evaluated by

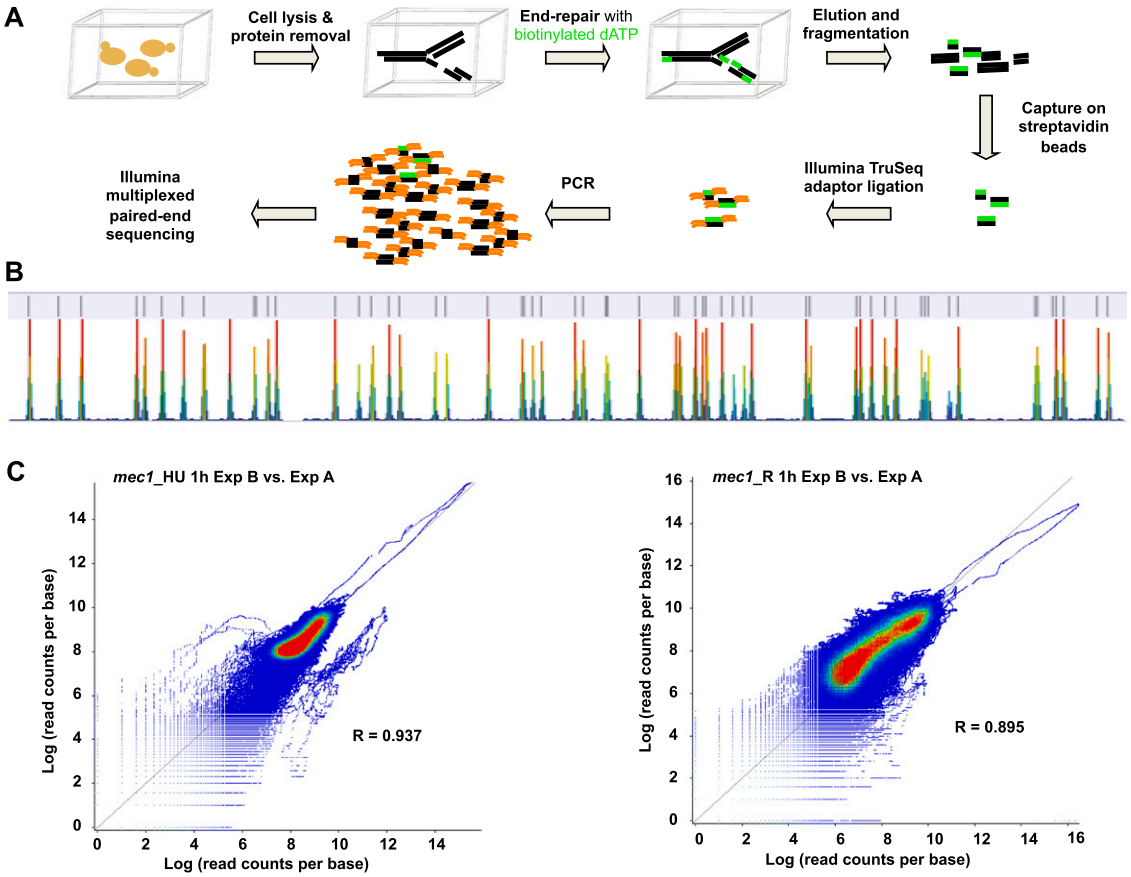

Figure 1. (*A*) Schematic representation of Break-seq procedures. Chromosomal DNA is shown embedded in agarose plugs (depicted by cubes) for in-gel labeling for DSBs. (*B*) View of a portion of Chromosome X (105,000–500,000 bp) showing the concordance between DSBs from the BamHI$^{mec1,\ G1}$ (control) sample and the known BamHI sites (the annotation track on *top*). The data track is shown at the *bottom*. Color scales from blue to red indicate increasing number of sequence reads in a given window. (*C*) Scatter plot of Pearson's correlation between two biological replicate experiments. Log transformed values of read counts per base normalized to total number of sequenced bases are plotted for the HU samples (*left*) and the Recovery samples (*right*). In each plot, the values from the Exp A samples are plotted on the *x*-axis and those from the Exp B samples on the *y*-axis.

calculating the frequency at which a randomized set of DSBs in a simulation (10,000 iterations) were found to overlap with origins at the same or greater frequency than the observed data. All three HU samples showed significant colocalization of the DSBs and origins ($P < 0.0001$). Thus, we concluded that low levels of chromosome breakage occurred near the origins even in the presence of HU in both *mec1* and *MEC1* cells. We note, however, that DSB signals near selected origins were at least partially attributable to ploidy increase.

DSBs during recovery from HU are correlated with replication fork progression

Using MACS, we also detected 190 and 217 DSBs in the Recovery^{mec1} samples from Exp A and B, respectively, with 65% concordance (Fig. 2B), and 79 DSBs in the Recovery^{MEC1} sample (Supplemental Table S4). DSBs during recovery from HU were more distal from the origins in the *MEC1* cells than those in the *mec1* cells (Fig. 2A), resulting in a lower concordance (R = 0.793) between DSBs in the HU and Recovery samples (Supplemental Table S3). This observation is consistent with the notion that in the *MEC1* cells, replication forks were capable of resuming after the removal of HU, whereas those in *mec1* cells were not (Feng et al. 2009). The comparison also revealed that at many genomic loci, the DSB level was only apparent in the Recovery sample compared to the HU sample (Fig. 2A).

Enrichment of chromosome breaks during recovery from HU occurs preferentially at transporter genes in *mec1* cells

We then asked if there were "enriched DSBs" in the Recovery samples relative to the HU samples by performing a Two-Sample test in MACS. We identified 186 and 209 enriched DSBs from Exp A and B, respectively, with ~50% overlap (Fig. 2C; Supplemental Table S5). The relatively low level of concordance is attributable to variations in replication fork dynamics as we previously observed unrestrained replication fork movement in *mec1* cells in HU (Feng et al. 2009). Nevertheless, we focused on those common regions of DSBs and asked: What makes these enriched DSBs the preferred sites for chromosome breakage?

We first examined what genomic features were associated with these enriched DSBs in the Recovery^{mec1} samples in the two biological replicate experiments. We identified 745 and 760 features in Exp A and B, respectively, either enclosed by or overlapping with the enriched DSBs (Fig. 2C). There were 203 common features, including 184 protein-coding genes, one pseudogene

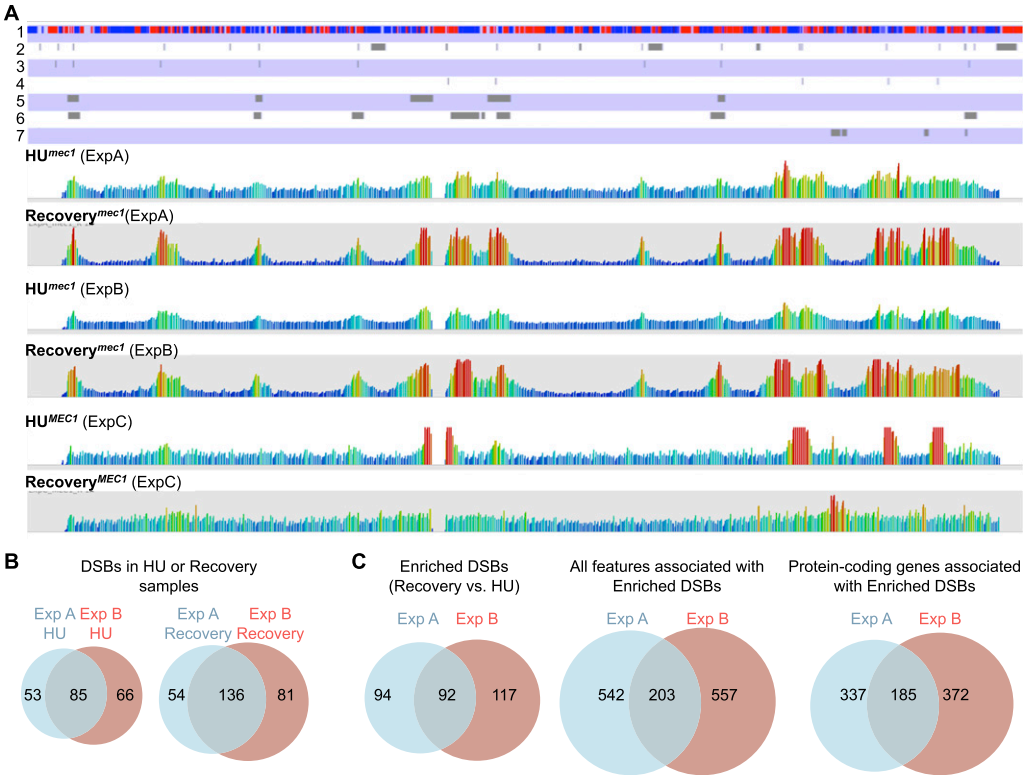

Figure 2. Chromosome views of the Break-seq data using SeqMonk. Sequence reads quantification was performed as described in Supplemental Figure S1. (*A*) View of Chromosome X (745,751 bp) of the HU and Recovery samples from all experiments. The annotation tracks from *top* to *bottom* are (1) ORFs (red, Watson-strand-encoded; blue, Crick-strand-encoded); (2) OriDB-curated confirmed and likely ARSs; (3) Rad53-checked origins (Feng et al. 2006); (4) Rad53-unchecked origins (Feng et al. 2006); (5) enriched DSBs in Exp A; (6) enriched DSBs in Exp B; and (7) enriched DSBs in Exp C. The data tracks are as labeled. (*B*) Venn diagrams showing concordance between the DSBs in HU samples alone and between the DSBs in Recovery samples alone in the two experiments. (*C*) Venn diagrams showing the concordance between the enriched DSBs in two experiments (*left*) and the identification of 203 common features (*middle*) and 185 common protein-coding genes (*right*).

(*YIL167W*, remnant of an ancestral ORF encoding an L-serine dehydratase found in other yeast species), 17 tRNAs, and one small nucleolar RNA (*SNR37*) associated with enriched DSBs (Fig. 2C; Supplemental Table S6). The RNA genes equally partitioned into convergent (nine tRNAs and *SNR37*) and codirectional (eight tRNAs) with respect to a replication fork from the nearest origin. In contrast, among the 185 common protein-coding genes, 69 are codirectional and 116 are convergent with the nearest replication fork (Supplemental Table S7). This bias for convergent replication and transcription contrasts the genome average—nearly equal numbers of ORFs in the yeast genome (3185 versus 3406) are convergent or codirectional with the nearest replication fork, respectively (χ^2 = 15.37, the two-tailed $P < 0.0001$). Therefore, we wondered if the formation of the enriched DSBs involved clashes between replication and transcription at these genes. If this were true, one would predict some commonality among these break-associated genes.

We then asked what Gene Ontology (GO) enrichment might exist among the 185 common genes, or "enriched DSB-associated genes." These genes were enriched for "transporter activity" (P = 0.0037) and consisted of a wide range of transporters of carbohydrates, lipids, metal ions, and drugs (Supplemental Table S8). In particular, "metal ion transmembrane transporter activity" (P = 0.002 and P = 0.004 for Exp A and B, respectively) was represented by 11 genes in each experiment, with four in common (*ARN2*, *YKE4*, *ALR2*, and *UGA4*, highlighted in Supplemental Table S8). These four gene products are responsible for transporting siderophore-iron, zinc, magnesium, and gamma-aminobutyric acid, respectively. The "enriched DSB-associated genes" also showed predominance for "salvage pathways of pyrimidine ribonucleotides" (*FUR1* and *CDD1*; P = 0.034). We note the observed GO enrichment was relatively weak, i.e., not deemed statistically significant ($P > 0.01$) when corrected for multiple testing. Nevertheless, we wondered whether the enrichment of DSBs associated with these genes was a result of transcription up-regulation in response to HU. Closer inspection of the enriched DSB loci provided evidence supporting our hypothesis. For instance, transcription from both *ARN2* and *UGA4* are convergent with replication from the nearest confirmed origin (Fig. 3A). Furthermore, we identified in both experiments an enriched DSB at Chr XII: 448345–451179, between the convergent *ARS1216* and the first copy of 35S rDNA transcript within the ribosomal DNA (rDNA) repeats (data not shown). Note the replication fork from *ARS1216* is not insulated by a replication fork barrier as are forks generated from the origins within the rDNA repeats.

Enriched DSBs in *MEC1* cells are correlated with transcription factors for stress response

We also identified 137 "enriched DSBs" from the Recovery^{MEC1} sample relative to the HU^{MEC1} sample in *MEC1* cells (Supplemental Table S5) and 244 associated genes (Supplemental Table S6). These genes were enriched for RNA polymerase II transcription factors

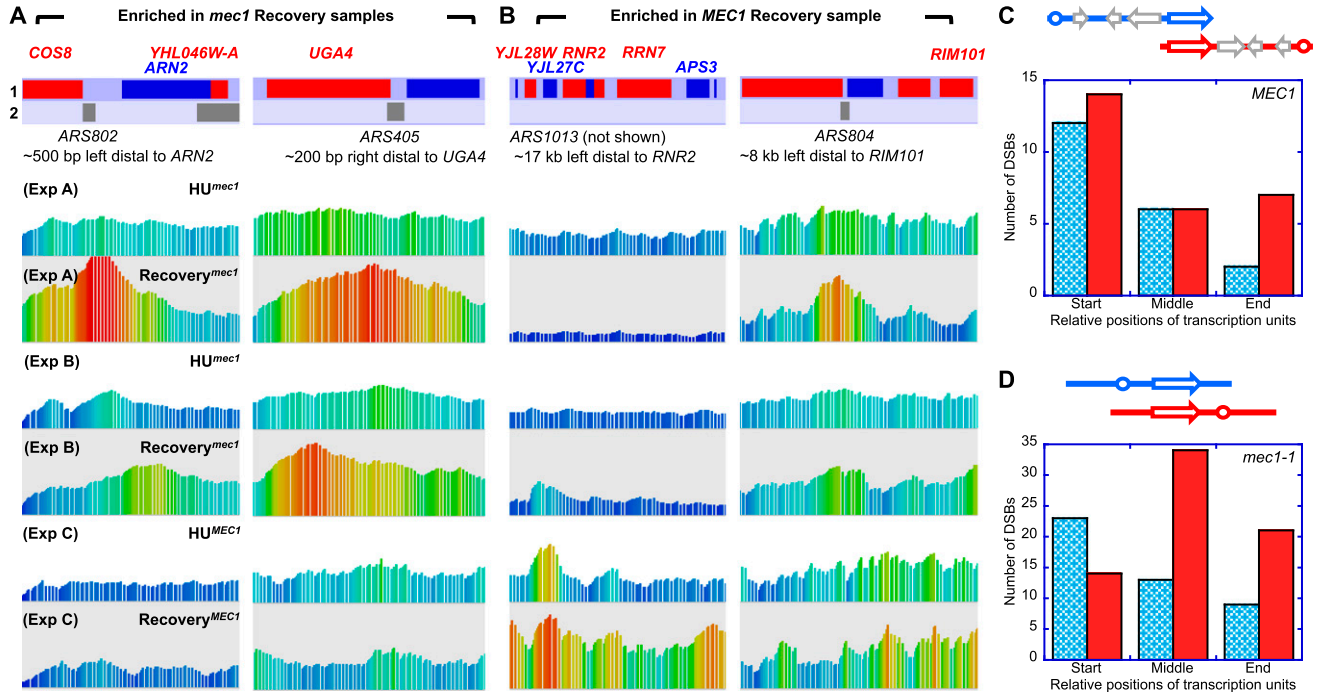

Figure 3. Examples of genomic loci containing enriched DSBs in *mec1* (*A*) and *MEC1* (*B*) cells. The annotation tracks are gene (1), labeled red and blue for Watson- and Crick-strand-encoded, respectively, and origins of replication (2). ORF names and ARS numbers are as labeled and *centered* on the marker in each track. The data tracks are as labeled. Only those genes that overlap with the enriched DSBs are named (*OCA5* and *WSC4* at the *ARS804* locus not shown). A dubious ORF and two tRNAs at the *RNR2* loci are not labeled due to space restriction. Distribution of enriched DSBs with respect to genes in *MEC1* (*C*) and *mec1* (*D*) cells. All DSB-associated genes, in either codirectional (blue) or convergent (red) orientation with respect to replication from the nearest origin (circles similarly color-coded in the two orientations) were aligned at the start codon and normalized by size. Genes (gray) in the intervening region between the origin and DSB-associated gene are illustrated to indicate the longer gene-to-origin distance in *MEC1* cells. The numbers of DSBs occurring at the relative positions of each gene were reported for the codirectional (blue) or convergent (red) groups in histograms.

(GO:1077; P = 0.005) (Supplemental Table S8), represented by *PDR3*, *RIM101*, *RPN4*, *UME6*, and *CAT8*, which are all direct or indirect regulators of stress response genes (Wendler et al. 1997; Nishizawa et al. 2010; Wang et al. 2010; Soontorngun et al. 2012; McDaniel and Strahl 2013). For instance, an enriched DSB-associated region ~15 kb downstream from *ARS1013* (Fig. 3B) encompasses *RNR2* (strongly induced by replication stress in a Mec1/Rad53 checkpoint-dependent manner) (Huang et al. 1998), *APS3* (encoding a small subunit of a clathrin-associated protein complex, whose protein abundance increases in response to DNA replication stress) (Tkach et al. 2012), *RRN7* (encoding a core factor of the rDNA transcriptional complex), and two uncharacterized ORFs (*YJL27C*, whose deletion renders the cell HU-sensitive, and *YJL28W*). Similarly, enriched DSBs were detected at the *RIM101* locus (Fig. 3B). In addition, distinct DSBs can also be observed—although not deemed significant by MACS—at *OCA5* and *WSC4,* both implicated in stress response (Verna et al. 1997). Interestingly, many of the targets of these stress-response genes were associated with enriched DSBs in the *mec1* mutant, e.g., *ARN2* and *YKE4* are substrates of *RIM101*, *RPN4*, and *UME6* (Salin et al. 2008; Reimand et al. 2010). Therefore, it stands to reason that a common stress response was elicited in the *mec1* and *MEC1* cells and that HU-induced gene expression causes unscheduled conflicts with replication at different loci contingent on replication fork progression.

We also asked whether the differential enrichment of DSB-associated genes in *MEC1* and *mec1* cells is due to nonrandom distribution of these genes with regard to their distance to origins. The average distance between the 113 most DSB-proximal genes (among the 244 genes encompassed by the enriched DSBs in the *MEC1* cells) and the nearest origin is 8649 bp (9476 bp if Rad53-checked origins were excluded), at least 3.3 times the average distance between the DSB-associated genes in *mec1* cells and their nearest origins (2619 bp). We asked if the transcription factors might be more distant from the origins than the transporter genes such that the replication forks in *mec1* cells would have a lower probability of encountering them during recovery from HU. The average distance between all 50 "RNA polymerase II transcription factors" [GO:1077] and their nearest origin is 7764 bp, and the average distance between 206 substrates of these transcription factors and their nearest origin is 7805 bp. We also tested multiple randomly chosen gene groups for origin-to-gene distances and did not find apparent bias for any group (data not shown). Thus, it does not appear that there is a biased distribution of yeast genes with regard to their relative location to the origins. That different DSB-associated genes are enriched in *mec1* versus *MEC1* cells is more likely due to differential replication dynamics, including origin activation timing/efficiencies and fork migration rates.

Meta-analyses of DSBs with regards to genes involved in codirectional or convergent replication and transcription

To gain a comprehensive understanding of the relationship between the enriched DSBs relative to the DSB-associated genes, we performed a meta-analysis to ask how the DSBs are distributed relative to the transcription unit. We calculated the relative dis-

tance between the center of each DSB and its associated gene—the actual distance (to the start, middle, and end of the gene) was normalized by gene size. In *MEC1* cells, DSBs tended to occur near the 5′-end of genes regardless of replication fork direction (Fig. 3C). However, there was a relatively increased proportion of DSBs near the 3′-end of genes when replication and transcription was convergent (Fig. 3C). In *mec1* cells, DSBs were similarly enriched near the 5′-end of genes in codirectional replication and transcription; however, there was a more significant shift of DSBs toward the middle and 3′-end of genes when replication and transcription were convergent.

RNA-seq reveals cell cycle phase-specific gene expression in *mec1* and *MEC1* cells

To further substantiate our core hypothesis, we examined global gene expression in cells under identical experimental conditions as for Break-seq, with the exception that two Recovery samples (R30 and R60, for 30 and 60 min of recovery, respectively) for each strain were collected (Fig. 4A). Flow cytometry analysis showed delayed replication progression during recovery in the *mec1* compared to the *MEC1* (WT) cells (Fig. 4B). Paired-end sequence reads from the mRNA libraries were quantified by RPKM (reads per kilobase per million reads) for every mRNA in the yeast genome (Supplemental Table S9). Those genes showing significant change ($P < 0.05$) between samples were identified (Supplemental Table S10). Hierarchical clustering analysis validated HU induction of genes from previously defined functional groups, including the Mec1 checkpoint-dependent DNA damage signature genes (Fig. 4C, left panel; Supplemental Table S10; Gasch et al. 2001; Dubacq et al. 2006). We then identified those genes with relatively higher expression in the Recovery than in the HU sample for both *MEC1* and *mec1* cells (Fig. 4C, middle and right panels; Supplemental Table S10). GO enrichment analysis demonstrated increased expression of oxidative stress response genes as exemplified by genes with oxidoreductase activities and those involved in cell wall structures in both *MEC1* and *mec1* cells (Supplemental Table S11). Moreover, *mec1* cells produced increased expression from iron binding genes [GO:5506] specifically during recovery, consistent with the observation that the enriched DSB-associated genes were predominantly metal ion transporter genes. Likewise, genes in the structural constituent of cell wall [GO:5199], comprised of *TIP1, SED1, CIS3, HSP150,* and *PIR1*, are all stress-response genes showing increased expression

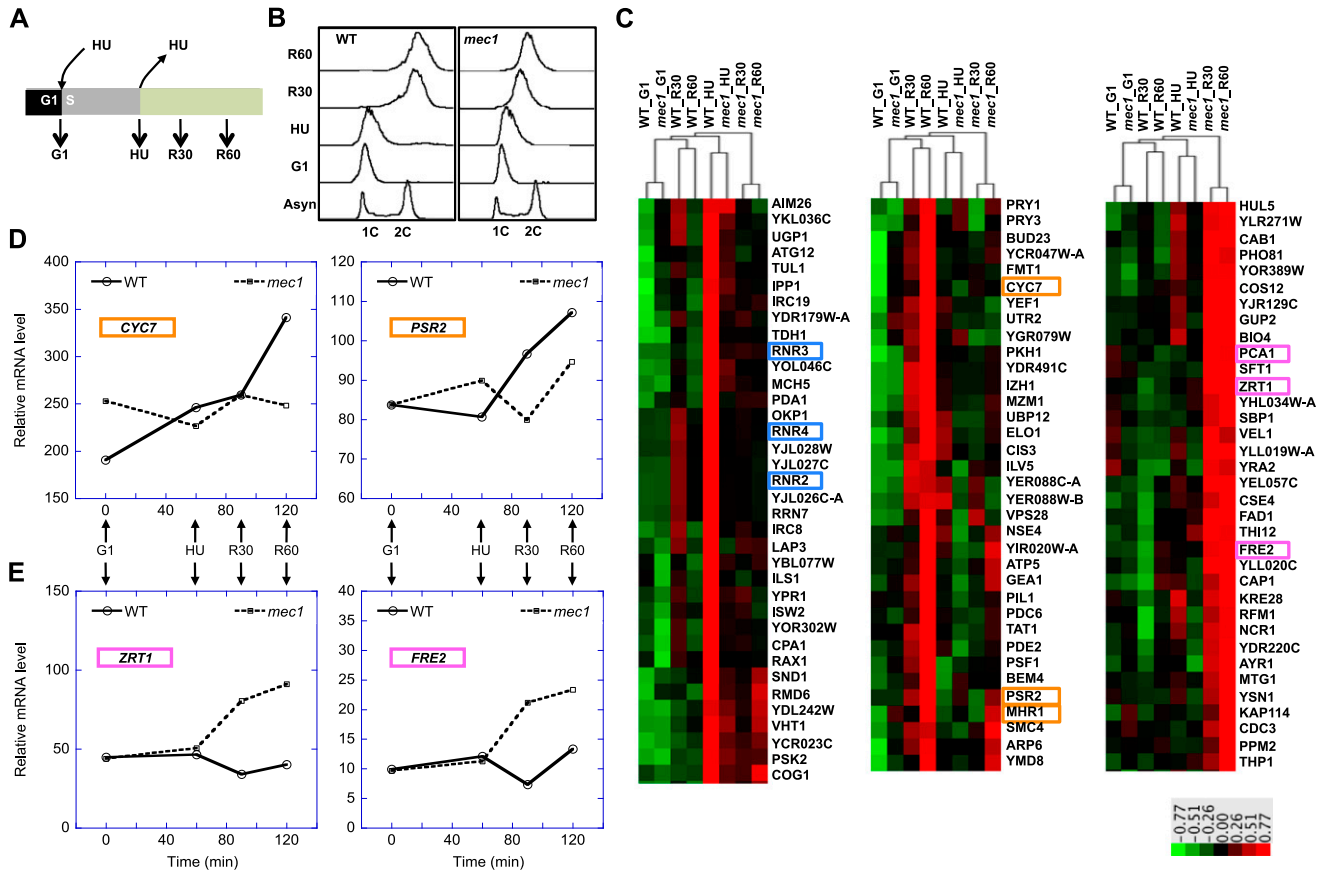

Figure 4. RNA-seq analysis. (*A*) Illustration of sample collection: (G1) α-factor arrested; (HU) exposed to HU for 1 h; (R30 and R60) recovery from HU for 30 and 60 min, respectively. (*B*) Cell cycle progression by FACS. (Asyn) Log phase culture prior to cell cycle synchronization. (*C*) Selected clusters of gene expression patterns in *MEC1* (WT) and *mec1* cells. Color bar values indicate $\log_{10}$ transformed values of normalized RPKM read count. The three panels represent growth phase- and strain-specific gene expression patterns. Selected genes in each cluster are boxed for emphasis and color-coded for the functional groups. (*Left*) HU-specific and Mec1-dependent (e.g., DNA damage response genes in blue boxes); (*middle*) Recovery-specific in WT cells (e.g., stress-response genes in orange boxes); (*right*) Recovery-specific in *mec1* cells (e.g., metal ion transporter genes in purple boxes). Gene expression profiles for selected Recovery-specific genes in WT (*D*) and *mec1* (*E*) cells from the cluster analysis are shown. The times at which the samples were taken are labeled on the time scale on the *x*-axes.

during recovery in *MEC1* cells (Supplemental Table S11). Temporal expression profiles of selected genes from these groups demonstrated recovery-specific expression in the respective strains (Fig. 4D,E). Therefore, these results recapitulated the enriched DSB patterns and provided support for our core hypothesis.

Chromosome breakage at the metal ion transporter genes is further enhanced by additional iron chelation in *mec1* cells recovering from HU

To further substantiate the hypothesis that HU-induced expression of metal ion transporter genes resulted in DSBs, we used bathophenanthroline sulfonate (BPS), an iron chelator, to further drive gene expression at the transporter genes in *mec1* cells. After the release from the G1/S transition and incubation with HU for 1 h, cells were allowed to recover with or without BPS for 1 h (*R-1h + BPS* and *R-1h − BPS*, respectively). First, we did not observe a significant difference at bulk levels of chromosome breakage in these samples by pulse field gel electrophoresis (Fig. 5A). Because DSBs were abundant, Break-chip offered sufficient sensitivity for this analysis. As shown in Figure 5B, higher levels of DSBs were observed at selected genomic regions in the sample with BPS than the one without BPS. We calculated the average signals in a 1-kb sliding window across the genome and identified those windows with a significant increase in the *R-1h + BPS* sample compared to the *R-1h − BPS* sample (>2 standard deviations, $P < 0.05$). We found 362 associated genes (Supplemental Table S12), including *ARN2* (encoding a siderophore transporter) and *GIN4* (encoding a protein kinase involved in bud growth and septin ring assembly) (Fig. 5B), both shown to be transcriptionally induced by iron deprivation (Yun et al. 2000; Protchenko et al. 2001; Shakoury-Elizeh et al. 2004; Puig et al. 2008). GO enrichment analysis revealed the following top categories, in descending order of significance: copper ion membrane transport [GO:35434] (P = 0.0001); copper ion import [GO:15677] (P = 0.0004); and mRNA export from nucleus in response to heat stress [GO:31990] (P = 0.0011). These genes are also enriched for iron ion homeostasis [GO:55072] (P = 0.0090). These results are consistent with our prediction that BPS treatment would further increase the transport of heavy metal ions across cellular membranes, thus supporting our hypothesis that DSBs can be enhanced by gene expression to increase the probability of conflicts with replication.

Programmed replication-transcription conflict through HU induction causes plasmid instability

To provide a more rigorous test of our hypothesis, we also asked whether HU produces chromosome instability in programmed convergent replication and transcription. We selected four genes, *YHK8, AHP1*, *RNR3*, and *TSA1*, previously shown to be induced by HU (Dubacq et al. 2006), as verified by RNA-seq (Supplemental Table S10). We cloned these genes and their endogenous promoters into a plasmid, YCpGal-ARS1-MCS, such that transcription would either occur toward (F) or away from (R) *ARS1*. We measured plasmid retention in *MEC1* cells exposed to HU for 1 h after synchronous entry into S phase, as well as in G1 control samples. The results indicated that placing these genes in convergent orientation with the incoming replication fork led to a greater reduction in plasmid stability compared to codirectional placement relative to the replication fork (P = 0.02 in a paired Student's t-test) (Fig. 6). These experiments provided further evidence that HU-induced convergent replication and transcription enhance chromosome fragility.

Discussion

Our previous studies have established that, after transient exposure to HU, checkpoint-deficient *mec1* cells suffer from extensive ssDNA formation and ultimately DSBs at destabilized replication forks (Feng et al. 2011). In this study, Break-seq analyses not only confirmed that chromosome breakage occurs at replication forks, but also provided evidence for enriched DSBs when cells attempted to recover from HU. The observations that enriched DSBs were associated with stress-response genes and with different subgroups represented in the *MEC1* and *mec1* cells led to a model for the mechanism of enhanced chromosome breakage during recovery from HU (Fig. 7). We propose that the enriched DSBs occurred at genomic loci where replication forks encountered transcription and/or transcription factor binding at HU-induced genes. Because the replication forks in *MEC1* cells were capable of traversing a greater distance after the removal of HU than those in *mec1* cells, different subclasses of the stress response genes were revealed in these cells. Consistent with the predictions from this model, we showed that further induction of the metal ion transporter genes through iron deprivation by BPS increased DSBs near these genes. We also provided evidence that programmed conflicts between replication and transcription induced by HU led to the reduction of plasmid stability, specifically when transcription occurred in a convergent manner with respect to replication. We acknowledge that there

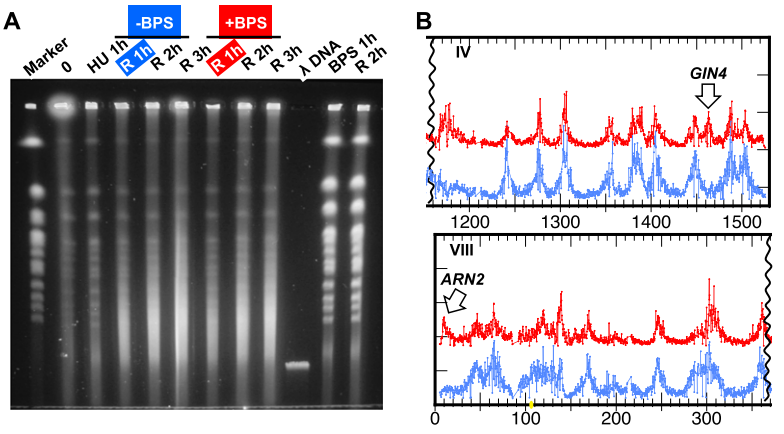

Figure 5. Treatment with BPS induces additional breakage at discrete loci. (*A*) Chromosome breakage is readily observed in *mec1* cells recovering from HU in the absence (blue, −BPS) and presence of 0.8 μM BPS (red, +BPS) by PFGE. BPS addition alone does not cause chromosome breakage: "BPS 1h" and "R 2h" represent cells that have been treated with BPS for 1 h and those that have recovered in fresh medium for 1 h after treatment with BPS, respectively. (Marker) Yeast chromosome PFG marker; (λ DNA) phage lambda DNA, ~50 kb. (*B*) Break-chip demonstrates examples of genomic regions showing enhanced breakage in the +BPS sample (red) compared to the –BPS sample (blue), as indicated by arrows.

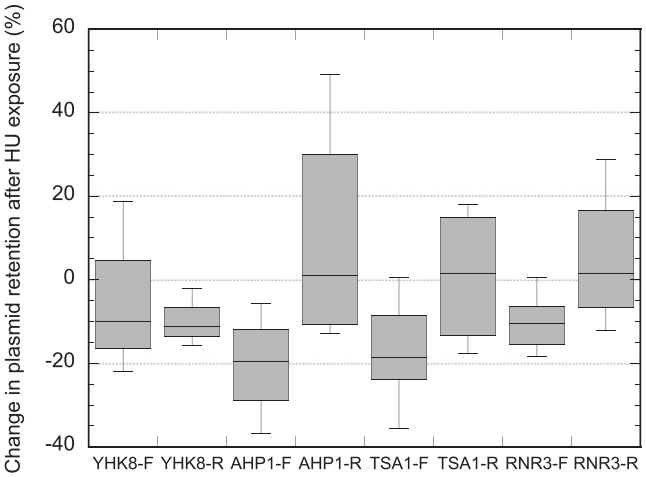

Figure 6. Replication and transcription in a convergent orientation cause higher levels of plasmid instability after HU induction than when in a codirectional orientation. Box plot of the percentages of change in plasmid stability in *MEC1* cells carrying *YHK8*, *AHP1*, *TSA1*, and *RNR3*, in either convergent (−F) or codirectional (−R) juxtaposition relative to the *ARS1* origin, after exposure to HU compared to the control (before exposure to HU) in a synchronous culture. Note that negative values denote *increased* plasmid *loss*. Each box encloses 50% of the data with the median value of the variable displayed as a line. The *top* and *bottom* of the box mark the upper and lower quartile (limits of ±25% of the variable population), respectively. The lines extending from the *top* and *bottom* of each box mark the minimum and maximum values within the data set.

is considerable variability in each Break-seq experiment with respect to the class of genes showing DSB association due to differential replication dynamics. Nevertheless, gene expression profiling provided support for the observed DSB patterns, as exemplified by the iron-binding genes enriched in *mec1* cells during recovery from HU.

Our hypothesis predicts that enriched DSBs (in recovery) would occur at genes normally expressed during S phase, such as the histone genes. To our surprise, histone genes were largely excluded from enriched DSBs despite the observation that the majority of canonical histone genes indeed showed S phase-specific expression, peaking at 30 min during recovery from HU (Supplemental Fig. S3A, B). Therefore, we entertained the possibility that replication might have preceded transcription at these loci, thus averting conflicts between replication and transcription. Indeed, based on a previous study (Alvino et al. 2007) at the cell cycle stage equivalent to the recovery phase in our experiments, the earliest-replicating histone genes (*HTA1/HTB1* and *HTA2/HTB2*) have achieved ~80% replication. On the other hand, the latest-replicating noncanonical histone gene loci (*HTZ1* and *HHO1*) were not transcriptionally induced (Supplemental Fig. S3C). Thus, both groups of genes were spared from replication-transcription conflict-induced DSBs. The *HHF1/HHT1* and *HHF2/HHT2* loci with intermediate replication timing and transcription induction comprised the only group that would show higher probability of coinciding replication and transcription. We did observe enriched DSBs in the vicinity of, albeit not within, these genes (data not shown). Therefore, it seems that the histone genes were largely exempted from DSBs due to temporally separated replication and transcription.

This work provided insights into the mechanisms of genome instability induced through replication-transcription conflicts. Meta-analysis of break positions within DSB-associated genes suggest that replication forks tend to stall at the 5′-end of genes regardless of fork direction in *MEC1* cells, albeit with a relative increase at the 3′-ends when replication and transcription were convergent. This biased DSB pattern was more pronounced in *mec1* cells—although codirectional replication and transcription still produced DSBs primarily at the 5′-ends of genes, convergent juxtaposition led to a more notable shift toward the middle and 3′-ends. These results suggest that replication forks were generally more unstable when encountering the transcription initiation complex than the termination complex in *MEC1* cells. In contrast, in *mec1* cells, convergent replication forks were more unstable when encountering the transcription elongation and/or termination complex. Alternatively, these biased DSB distributions might reflect the patterns of residual stalled transcription initiation or elongation complex from G1 persisting into subsequent stages of the cell cycle. Our observations in *MEC1* yeast cells therefore contrasted the "punctuation mark theory" based on bacterial plasmids in which the transcription initiation complex preferentially stalls the convergent replication fork, whereas the termination complex preferentially stalls the codirectional replication fork (Mirkin et al. 2006). This apparent discrepancy might reflect intrinsic differences between a functional transcription complex in our system versus an engineered and stationary complex in bacteria. Alternatively, differences in replication fork speed and/or replicative helicase polarities between these two organisms might also contribute to these results. Future work is warranted to investigate the cause for the positional bias of replication fork stalling within a transcription unit in yeast.

Our work also bears on our understanding of HU's impact on cellular processes. Although HU is primarily known as a ribonucleotide reductase inhibitor, it has a multitude of other cellular effects. For instance, HU treatment results in lowered intracellular iron and in turn, increased iron uptake by transferrin (Chitambar and Wereley 1995). HU has also been shown to bind metal ions such as iron and copper directly (Konstantinou et al. 2011). Moreover, HU induces oxidative stress response (Dubacq et al. 2006). Cellular defense against oxidative stress requires the activities of superoxide dismutases (SODs), which in turn require increased mobilization of heavy metals across different cellular membranes for their activities toward reactive oxygen species: copper and zinc for Sod1 (Bermingham-McDonogh et al. 1988; Chang et al. 1991) and manganese for Sod2 (Ravindranath and Fridovich 1975). Finally, we have also uncovered diverse chemical-genetic interactions between HU and a wide range of genetic mutants (McCulley et al. 2014). Therefore, we propose that HU triggers a global stress response involving proteins with a wide range of cellular functions, including heavy metal mobilization.

In summary, we have upgraded Break-chip to Break-seq with superior sensitivity of DSB detection. This improvement facilitated the discovery of enriched DSBs in cells recovering from exposure to HU compared to cells whose cell cycle was still arrested by the drug and led to the hypothesis that unscheduled conflict between replication and transcription underlies replication stress-induced chromosome breakage. Our model potentially provides a solution to a long-standing problem in mammalian chromosome biology: The reason why replication inhibitors induce distinct patterns of CFSs is because they each produce a different gene expression pattern and cause replication-transcription conflicts at different genomic regions. This work also explains why chromosome breakage was more pronounced in the Recovery than in the HU sample: In HU, replication forks stall and have a lower probability

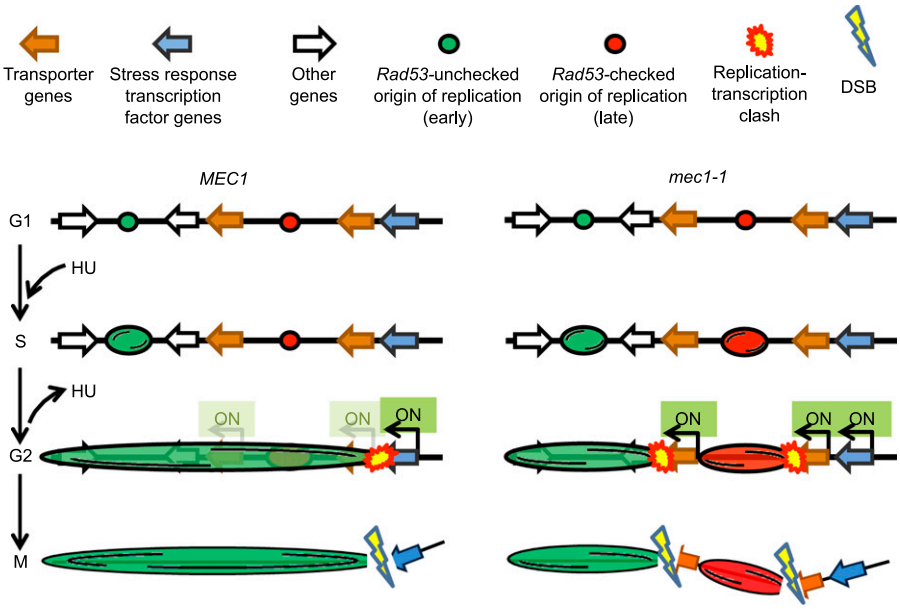

Figure 7. Model for chromosome fragility induced by HU as a result of unscheduled conflict between destabilized replication forks and increased gene transcription at HU-inducible genes in *mec1* cells and *MEC1* cells. In the presence of HU only those Rad53-unchecked origins (Feng et al. 2006) are activated in *MEC1* cells and the replication forks travel a greater distance than those in the *mec1* cells, thus reaching different locations in the genome. Therefore, during recovery from HU, the stalled replication forks in *MEC1* and *mec1* cells encounter the transcription induction of different subsets of HU-responsive genes. Collision between replication and transcription brings forth further destabilization of the ssDNA at the replication forks, causing DSBs. Note that although the replication forks in WT cells would have traversed through the HU-induced genes that are proximal to the origins observed in the *mec1* cells, ssDNA is only formed at the replication fork at a more distal region, thus sparing these genes from DSBs.

of breaking and colliding with transcription, whereas during recovery they can resume or initiate from the previously unfired origins, thus increasing the probability of DSBs. We believe that the Break-seq methodology as well as our proposed model of chromosome breakage will have direct impact on the discovery of mammalian chromosome fragile sites.

Methods

Yeast growth conditions and strains

All yeast strains were cultured in YPD medium or SC medium lacking tryptophan and incubated at 30°C. The strains used in this study were derivatives of strain A364a: WFA72; *MATa leu2-3,112 trp1-1 his3-11* and WFA73; *MATa mec1-1::HIS3 sml1-1 leu2-3,112 trp1-1 his3-11*.

Cell cycle synchronization, sample collection, and preparation of agarose-embedded chromosomal DNA

Cells were grown in YPD liquid medium at 30°C until they reached an optical density at 600 nm (OD_{600}) of ~0.25. The cultures were then synchronized by 3 μM α-factor, followed by release into S phase with pronase addition (0.3 μg/mL). HU was added at 200 mM immediately before adding pronase. After 1 h, cultures were filtered to remove HU and cells were resuspended in fresh YPD medium to recover for up to 3 h with samples taken every hour. BPS was added at 0.8 μM to the YPD medium just before cell resuspension. Approximately 10^6 yeast cells from each sample were washed in 50 mM EDTA and embedded in 0.5% Incert low-melting agarose (Lonza) in 50 mM EDTA, then cast in a 100-μL mold (Bio-Rad) to solidify. The plugs were then processed for cell lysis and protein removal as previously described (Feng et al. 2011).

Flow cytometric analysis

One-milliliter samples from the synchronized cultures described above were collected every 15 min and fixed with ethanol. SYTOX green-stained samples were measured for DNA content with a Beckton Dickinson LSRFortessa. Data analysis was performed with FlowJo.

Pulse field gel electrophoresis

PFGE analysis was performed as described previously (van Brabant et al. 2001). Electrophoresis was conducted for 24 h at 14°C with a switch time ramped from 10 to 90 sec at 6 volts/cm. Standard procedures were used to ethidium bromide stain and photograph the gel.

Cloning of *AHP1, TSA1, YHK8,* and *RNR3*

PCR products of *AHP1*, *TSA1*, *YHK8*, and *RNR3*, along with flanking sequences, were cloned into YCpGal-ARS1-MCS, derived from YCpGal-ARS1 (MK Raghuraman, unpubl.), replacing a *GAL1* promoter adjacent to the origin, *ARS1*, such that transcription occurs either toward (Forward, "F") or away from (Reverse, "R") *ARS1*. The PCR products were inserted as either NdeI-NotI (*AHP1*) or AseI-NotI (all others) fragments into the NdeI and NotI sites. PCR primer sequences are listed in Supplemental Table S13. All clones were confirmed by Sanger sequencing.

Plasmid retention assay

WFA72 cells transformed with plasmids described above were grown in synthetic medium lacking tryptophan (SC-Trp) at 30°C until OD_{600} reached ~0.25. Cell cycle synchronization and HU (200 mM) treatment were performed as described above. After 1 h treatment, serial diluted cells were plated at ~500 cells per plate on solid YPD or SC-Trp medium after sonication, and plates were incubated for 2–3 d at 30°C before colonies were counted. The percentage of plasmid retention was calculated as the percentage of tryptophan prototrophic colonies of total number of colonies on YPD medium. Each measurement was averaged from at least three biological replicates.

Break-seq and data analyses

Agarose-embedded chromosomal DNA samples were subjected to Break-seq library construction. Detailed procedures as well as sequence data analyses, including the random simulation tests, are described in the Supplemental Material.

Break-chip

DSB labeling followed by sample hybridization on Agilent G4493A Yeast Whole Genome ChIP-on-Chip 4 × 44K microarrays were performed as previously described with one modification (Feng

et al. 2011). Extraction of DNA from agarose plugs was performed by β-agarase digestion rather than electroelution described in the Break-seq procedures.

RNA-seq

Total RNA was isolated from ~5×10^8 cells by standard procedure, and 2 μg of RNA from each sample was used to prepare mRNA libraries using the Illumina TruSeq Stranded mRNA Sample Preparation Kit according to the manufacturer's recommendations. The libraries were validated on the Agilent Technologies 2100 Bioanalyzer using the Agilent DNA 1000 chip, pooled and sequenced on the MiSeq using a 2 × 75 cycle run. Raw sequences were mapped onto the SacCer3 genome by BWA and subsequent analyses were performed with SeqMonk and Cluster 3.0 (de Hoon et al. 2004). Java TreeView (Saldanha 2004) was used to visualize clustered data.

Gene ontology (GO) enrichment analysis

All data analysis of GO enrichment for either molecular function or biological process was performed with the *Saccharomyces cerevisiae* genome database "Gene Ontology Enrichment" widget, or by using FunSpec (Robinson et al. 2002) with a maximum *P*-value of 0.01. For RNA-seq data, GO enrichment *P*-values were corrected for multiple testing by the Benjamini-Hochberg method (Hochberg and Benjamini 1990).

Data access

All primary sequencing data from this study have been submitted to the NCBI Gene Expression Omnibus (GEO; http://www.ncbi.nlm.nih.gov/geo/) under the SuperSeries accession GSE63517, with the Break-seq, RNA-seq, and Break-chip data assigned separate accession numbers, GSE58808, GSE63516, and GSE64446, respectively.

Acknowledgments

We wish to thank Anna Brosius for sharing shell scripts for bwa sequence mapping and analysis; Sujith Valiyaparambil and Jonathan Bard at the University at Buffalo Genomics and Bioinformatics Core for HiSeq sequencing; Siyi Zhang and Jie Peng for assisting data analysis; and Nancy Walker for technical support. We are also indebted to Karen Gentile and Frank Middleton at Upstate Medical University Microarray and Sequencing Core Facility for generous help with MiSeq sequencing. We also thank M.K. Raghuraman and Sara Di Rienzi for critical reading of the manuscript. This work was supported by a Pathway to Independence Award (4R00GM08137804) from the National Institutes of Health and a Basil O'Connor Starter Scholar Award (56464) from March of Dimes to W.F.

References

Alvino GM, Collingwood D, Murphy JM, Delrow J, Brewer BJ, Raghuraman MK. 2007. Replication in hydroxyurea: it's a matter of time. *Mol Cell Biol* **27:** 6396–6406.

Arlt MF, Durkin SG, Ragland RL, Glover TW. 2006. Common fragile sites as targets for chromosome rearrangements. *DNA Repair (Amst)* **5:** 1126–1135.

Azvolinsky A, Giresi PG, Lieb JD, Zakian VA. 2009. Highly transcribed RNA polymerase II genes are impediments to replication fork progression in *Saccharomyces cerevisiae*. *Mol Cell* **34:** 722–734.

Bermejo R, Lai MS, Foiani M. 2012. Preventing replication stress to maintain genome stability: resolving conflicts between replication and transcription. *Mol Cell* **45:** 710–718.

Bermingham-McDonogh O, Gralla EB, Valentine JS. 1988. The copper, zinc-superoxide dismutase gene of *Saccharomyces cerevisiae*: cloning, sequencing, and biological activity. *Proc Natl Acad Sci* **85:** 4789–4793.

Brewer BJ. 1988. When polymerases collide: replication and the transcriptional organization of the *E. coli* chromosome. *Cell* **53:** 679–686.

Brewer BJ, Fangman WL. 1988. A replication fork barrier at the 3′ end of yeast ribosomal RNA genes. *Cell* **55:** 637–643.

Casper AM, Rosen DM, Rajula KD. 2012. Sites of genetic instability in mitosis and cancer. *Ann NY Acad Sci* **1267:** 24–30.

Chang EC, Crawford BF, Hong Z, Bilinski T, Kosman DJ. 1991. Genetic and biochemical characterization of Cu,Zn superoxide dismutase mutants in *Saccharomyces cerevisiae*. *J Biol Chem* **266:** 4417–4424.

Chitambar CR, Wereley JP. 1995. Effect of hydroxyurea on cellular iron metabolism in human leukemic CCRF-CEM cells: changes in iron uptake and the regulation of transferrin receptor and ferritin gene expression following inhibition of DNA synthesis. *Cancer Res* **55:** 4361–4366.

de Hoon MJ, Imoto S, Nolan J, Miyano S. 2004. Open source clustering software. *Bioinformatics* **20:** 1453–1454.

Debatisse M, Le Tallec B, Letessier A, Dutrillaux B, Brison O. 2012. Common fragile sites: mechanisms of instability revisited. *Trends Genet* **28:** 22–32.

Deshpande AM, Newlon CS. 1996. DNA replication fork pause sites dependent on transcription. *Science* **272:** 1030–1033.

Dubacq C, Chevalier A, Courbeyrette R, Petat C, Gidrol X, Mann C. 2006. Role of the iron mobilization and oxidative stress regulons in the genomic response of yeast to hydroxyurea. *Mol Genet Genomics* **275:** 114–124.

Duch A, Felipe-Abrio I, Barroso S, Yaakov G, García-Rubio M, Aguilera A, de Nadal E, Posas F. 2013. Coordinated control of replication and transcription by a SAPK protects genomic integrity. *Nature* **493:** 116–119.

Durkin SG, Glover TW. 2007. Chromosome fragile sites. *Annu Rev Genet* **41:** 169–192.

Feng W, Collingwood D, Boeck ME, Fox LA, Alvino GM, Fangman WL, Raghuraman MK, Brewer BJ. 2006. Genomic mapping of single-stranded DNA in hydroxyurea-challenged yeasts identifies origins of replication. *Nat Cell Biol* **8:** 148–155.

Feng W, Bachant J, Collingwood D, Raghuraman MK, Brewer BJ. 2009. Centromere replication timing determines different forms of genomic instability in *Saccharomyces cerevisiae* checkpoint mutants during replication stress. *Genetics* **183:** 1249–1260.

Feng W, Di Rienzi SC, Raghuraman MK, Brewer BJ. 2011. Replication stress-induced chromosome breakage is correlated with replication fork progression and is preceded by single-stranded DNA formation. *G3 (Bethesda)* **1:** 327–335.

Gasch AP, Huang M, Metzner S, Botstein D, Elledge SJ, Brown PO. 2001. Genomic expression responses to DNA-damaging agents and the regulatory role of the yeast ATR homolog Mec1p. *Mol Biol Cell* **12:** 2987–3003.

Hellman A, Rahat A, Scherer SW, Darvasi A, Tsui LC, Kerem B. 2000. Replication delay along FRA7H, a common fragile site on human chromosome 7, leads to chromosomal instability. *Mol Cell Biol* **20:** 4420–4427.

Hochberg Y, Benjamini Y. 1990. More powerful procedures for multiple significance testing. *Stat Med* **9:** 811–818.

Huang M, Zhou Z, Elledge SJ. 1998. The DNA replication and damage checkpoint pathways induce transcription by inhibition of the Crt1 repressor. *Cell* **94:** 595–605.

Konstantinou E, Pashalidis I, Kolnagou A, Kontoghiorghes GJ. 2011. Interactions of hydroxycarbamide (hydroxyurea) with iron and copper: implications on toxicity and therapeutic strategies. *Hemoglobin* **35:** 237–246.

Langmead B, Salzberg SL. 2012. Fast gapped-read alignment with Bowtie 2. *Nat Methods* **9:** 357–359.

Le Beau MM, Rassool FV, Neilly ME, Espinosa R III, Glover TW, Smith DI, McKeithan TW. 1998. Replication of a common fragile site, FRA3B, occurs late in S phase and is delayed further upon induction: implications for the mechanism of fragile site induction. *Hum Mol Genet* **7:** 755–761.

Letessier A, Millot GA, Koundrioukoff S, Lachagès AM, Vogt N, Hansen RS, Malfoy B, Brison O, Debatisse M. 2011. Cell-type-specific replication initiation programs set fragility of the *FRA3B* fragile site. *Nature* **470:** 120–123.

Li H, Durbin R. 2009. Fast and accurate short read alignment with Burrows-Wheeler transform. *Bioinformatics* **25:** 1754–1760.

Luna R, Rondón AG, Aguilera A. 2012. New clues to understand the role of THO and other functionally related factors in mRNP biogenesis. *Biochim Biophys Acta* **1819:** 514–520.

MacAlpine DM, Bell SP. 2005. A genomic view of eukaryotic DNA replication. *Chromosome Res* **13:** 309–326.

McCulley A, Haarer B, Viggiano S, Karchin J, Feng W. 2014. Chemical suppression of defects in mitotic spindle assembly, redox control, and sterol biosynthesis by hydroxyurea. *G3 (Bethesda)* **4:** 39–48.
McDaniel SL, Strahl BD. 2013. Stress-free with Rpd3: a unique chromatin complex mediates the response to oxidative stress. *Mol Cell Biol* **33:** 3726–3727.
Merrikh H, Zhang Y, Grossman AD, Wang JD. 2012. Replication-transcription conflicts in bacteria. *Nat Rev Microbiol* **10:** 449–458.
Mirkin EV, Mirkin SM. 2007. Replication fork stalling at natural impediments. *Microbiol Mol Biol Rev* **71:** 13–35.
Mirkin EV, Castro Roa D, Nudler E, Mirkin SM. 2006. Transcription regulatory elements are punctuation marks for DNA replication. *Proc Natl Acad Sci* **103:** 7276–7281.
Murano I, Kuwano A, Kajii T. 1989. Fibroblast-specific common fragile sites induced by aphidicolin. *Hum Genet* **83:** 45–48.
Nieduszynski CA, Hiraga S, Ak P, Benham CJ, Donaldson AD. 2007. OriDB: a DNA replication origin database. *Nucleic Acids Res* **35:** D40–D46.
Nishizawa M, Tanigawa M, Hayashi M, Maeda T, Yazaki Y, Saeki Y, Toh-e A. 2010. Pho85 kinase, a cyclin-dependent kinase, regulates nuclear accumulation of the Rim101 transcription factor in the stress response of *Saccharomyces cerevisiae*. *Eukaryot Cell* **9:** 943–951.
Ozeri-Galai E, Lebofsky R, Rahat A, Bester AC, Bensimon A, Kerem B. 2011. Failure of origin activation in response to fork stalling leads to chromosomal instability at fragile sites. *Mol Cell* **43:** 122–131.
Palakodeti A, Han Y, Jiang Y, Le Beau MM. 2004. The role of late/slow replication of the FRA16D in common fragile site induction. *Genes Chromosomes Cancer* **39:** 71–76.
Pomerantz RT, O'Donnell M. 2010. Direct restart of a replication fork stalled by a head-on RNA polymerase. *Science* **327:** 590–592.
Protchenko O, Ferea T, Rashford J, Tiedeman J, Brown PO, Botstein D, Philpott CC. 2001. Three cell wall mannoproteins facilitate the uptake of iron in *Saccharomyces cerevisiae*. *J Biol Chem* **276:** 49244–49250.
Puig S, Vergara SV, Thiele DJ. 2008. Cooperation of two mRNA-binding proteins drives metabolic adaptation to iron deficiency. *Cell Metab* **7:** 555–564.
Ravindranath SD, Fridovich I. 1975. Isolation and characterization of a manganese-containing superoxide dismutase from yeast. *J Biol Chem* **250:** 6107–6112.
Reimand J, Vaquerizas JM, Todd AE, Vilo J, Luscombe NM. 2010. Comprehensive reanalysis of transcription factor knockout expression data in *Saccharomyces cerevisiae* reveals many new targets. *Nucleic Acids Res* **38:** 4768–4777.
Robinson MD, Grigull J, Mohammad N, Hughes TR. 2002. FunSpec: a web-based cluster interpreter for yeast. *BMC Bioinformatics* **3:** 35.
Rocha E. 2002. Is there a role for replication fork asymmetry in the distribution of genes in bacterial genomes? *Trends Microbiol* **10:** 393–395.
Saldanha AJ. 2004. Java Treeview—extensible visualization of microarray data. *Bioinformatics* **20:** 3246–3248.
Salin H, Fardeau V, Piccini E, Lelandais G, Tanty V, Lemoine S, Jacq C, Devaux F. 2008. Structure and properties of transcriptional networks driving selenite stress response in yeasts. *BMC Genomics* **9:** 333.
Shakoury-Elizeh M, Tiedeman J, Rashford J, Ferea T, Demeter J, Garcia E, Rolfes R, Brown PO, Botstein D, Philpott CC. 2004. Transcriptional remodeling in response to iron deprivation in *Saccharomyces cerevisiae*. *Mol Biol Cell* **15:** 1233–1243.
Soontorngun N, Baramee S, Tangsombatvichit C, Thepnok P, Cheevadhanarak S, Robert F, Turcotte B. 2012. Genome-wide location analysis reveals an important overlap between the targets of the yeast transcriptional regulators Rds2 and Adr1. *Biochem Biophys Res Commun* **423:** 632–637.
Sutherland GR. 1979. Heritable fragile sites on human chromosomes. III. Detection of fra(X)(q27) in males with X-linked mental retardation and in their female relatives. *Hum Genet* **53:** 23–27.
Tkach JM, Yimit A, Lee AY, Riffle M, Costanzo M, Jaschob D, Hendry JA, Ou J, Moffat J, Boone C, et al. 2012. Dissecting DNA damage response pathways by analysing protein localization and abundance changes during DNA replication stress. *Nat Cell Biol* **14:** 966–976.
Tuduri S, Crabbé L, Conti C, Tourrière H, Holtgreve-Grez H, Jauch A, Pantesco V, De Vos J, Thomas A, Theillet C, et al. 2009. Topoisomerase I suppresses genomic instability by preventing interference between replication and transcription. *Nat Cell Biol* **11:** 1315–1324.
van Brabant AJ, Buchanan CD, Charboneau E, Fangman WL, Brewer BJ. 2001. An origin-deficient yeast artificial chromosome triggers a cell cycle checkpoint. *Mol Cell* **7:** 705–713.
Verna J, Lodder A, Lee K, Vagts A, Ballester R. 1997. A family of genes required for maintenance of cell wall integrity and for the stress response in *Saccharomyces cerevisiae*. *Proc Natl Acad Sci* **94:** 13804–13809.
Wang L, Darling J, Zhang JS, Qian CP, Hartmann L, Conover C, Jenkins R, Smith DI. 1998. Frequent homozygous deletions in the FRA3B region in tumor cell lines still leave the FHIT exons intact. *Oncogene* **16:** 635–642.
Wang X, Xu H, Ha SW, Ju D, Xie Y. 2010. Proteasomal degradation of Rpn4 in *Saccharomyces cerevisiae* is critical for cell viability under stressed conditions. *Genetics* **184:** 335–342.
Wendler F, Bergler H, Prutej K, Jungwirth H, Zisser G, Kuchler K, Högenauer G. 1997. Diazaborine resistance in the yeast *Saccharomyces cerevisiae* reveals a link between *YAP1* and the pleiotropic drug resistance genes *PDR1* and *PDR3*. *J Biol Chem* **272:** 27091–27098.
Yin S, Deng W, Hu L, Kong X. 2009. The impact of nucleosome positioning on the organization of replication origins in eukaryotes. *Biochem Biophys Res Commun* **385:** 363–368.
Yun CW, Ferea T, Rashford J, Ardon O, Brown PO, Botstein D, Kaplan J, Philpott CC. 2000. Desferrioxamine-mediated iron uptake in *Saccharomyces cerevisiae*. Evidence for two pathways of iron uptake. *J Biol Chem* **275:** 10709–10715.
Zhang Y, Liu T, Meyer CA, Eeckhoute J, Johnson DS, Bernstein BE, Nusbaum C, Myers RM, Brown M, Li W, et al. 2008. Model-based analysis of ChIP-Seq (MACS). *Genome Biol* **9:** R137.

Received June 25, 2014; accepted in revised form January 12, 2015.